

The Molecular Accretion Flow in G10.6-0.4

Peter K. Sollins, Paul T. P Ho

*Harvard-Smithsonian Center for Astrophysics, 60 Garden Street, Cambridge, MA, 02138,
psollins@cfa.harvard.edu*

ABSTRACT

We have observed the ultracompact HII region G10.6-0.4 with the VLA in 23 GHz continuum and the $\text{NH}_3(3,3)$ inversion line. By analyzing the optical depth of the line as well as the kinematics, we have detected a flattened, rotating, molecular accretion flow. We detect the fact that the highest column density gas is more flattened, that is, distributed more narrowly, than the lower column density gas, and that there is some inclination of the rotation axis. The rotation is sub-Keplerian, and the molecular gas is not in a rotationally supported disk. We do not find a single massive (proto)star forming in a scaled up version of low mass star formation. Instead, our observations suggest a different mode of clustered massive star formation, in which the accretion flow flattens but does not form an accretion disk. Also in this mode of star formation the central object can be a group of massive stars rather than a single massive star.

Subject headings: stars: formation — ISM: individual (G10.6-0.4) — HII regions — accretion

1. Introduction

G10.6-0.4 is a bright, 2.5 Jy at 23 GHz (Keto et al. 1987a), ultra-compact (UC) HII region (Wood & Churchwell 1989) at a distance of 6.0 kpc (Downes et al. 1980), in an area of active star formation. The associated *IRAS* point source, *IRAS* 18075-1956, has a luminosity of $9.2 \times 10^5 L_\odot$ (Casoli et al. 1986) and has colors that meet the criteria of Wood & Churchwell (1989) for an UCHII region. G10.6 is known to be embedded in a hot molecular core (HMC) (Braz & Epchtein 1983; Ho & Haschick 1986; Plume et al. 1992). The core is thought to contain 1200 M_\odot of gas within a radius of 0.2 pc, based on an analysis of a variety of dust continuum measurements (Mueller et al. 2002), and 3300 M_\odot within 1.1 pc based on C^{18}O and C^{17}O measurements (Hofner et al. 2000). Previous studies of the inversion lines of NH_3 have determined that the molecular core is rotating and collapsing

inward toward the UCHII region (Ho & Haschick 1986; Keto et al. 1987b, 1988; Keto 1990). In these studies, using the $\text{NH}_3(1,1)$ and $\text{NH}_3(3,3)$ lines, rotation is seen at size scales from 1 pc down to 0.08 pc, and infall is detected in the form of red-shifted absorption seen against the continuum source. CH_3OH and H_2O masers are seen distributed linearly in the plane of the rotation (Walsh et al. 1998; Hofner & Churchwell 1996), while OH masers seem to lie along the axis of rotation (Argon et al. 2000). In C^{18}O ($J = 1 \rightarrow 0$), Ho et al. (1994) see $10^3 M_\odot$ of dense ($n \sim 10^6 \text{cm}^{-3}$), rotating gas in a flattened (0.3×0.1 pc) disk-like structure. At the highest resolution achieved in earlier work, infall and rotation in the molecular gas were seen simultaneously in absorption, showing that the molecular gas was spiraling inward on size scales comparable to the size of the UCHII region.

Recent observations of G10.6 hinted that it might represent a previously unobserved mode of high mass star formation. Observations of $\text{H}66\alpha$ from the ionized gas within the UCHII region indicate that the ionized gas is also spiraling inward toward the stars at the center of the UCHII region (Keto 2002a). Subsequent theoretical work showed that in small HII regions, the gravitational effect of the central star(s) can overcome the thermal pressure of the ionized gas causing the molecular accretion flow to pass through the HII region boundary and continue inward as an ionized accretion flow (Keto 2002b). In this model, the HII region boundary exists as a standing R-type ionization front within a continuous accretion flow. These results differ from classical treatments of the pressure driven expansion of HII regions, which predict outward motion of the ionized gas as soon as the HII region is formed (Strömgren 1939; Spitzer 1978). In the classical model for pressure driven expansion, the HII region boundary, after a very short phase as a moving R-type front, will develop a characteristic double front structure composed of an isothermal shock followed by a moving D-type ionization front. As the HII region expands, most of the displaced molecular material remains between the shock and the ionization front as a dense outward moving shell, which snow-plows ahead of the HII region. If, however, the accretion flow passes through a standing R-type ionization front at the HII region boundary and continues toward the star(s) as an ionized flow, as suggested by Keto (2002b), there will be no dense molecular layer at the boundary, and all the molecular gas will be moving inward.

Sollins et al. (2005) did preliminary analysis of the data presented here, and showed that G10.6 is accreting through its UCHII region. The velocities of the molecular gas showed clear evidence of both infall and rotation. Based on geometrical arguments, Sollins et al. (2005) concluded that the infalling layer proceeded directly up to the ionization front. They also showed a non-detection of any expanding molecular gas. The non-detection placed such a stringent upper limit on the mass of any expanding molecular shell that might be present, that it was concluded that no such expansion was taking place, and that the accretion in the ionized and molecular gas were all part of a single accretion flow which continues across

a stalled ionization front.

In this paper we present a more detailed analysis of the NH_3 data. We conclude that, while the accretion flow is spherical at large radii, the rotation does cause it to flatten somewhat on the size scale of the UCHII region, so that the highest column densities appear in a thin strip. We also conclude that the axis of rotation is inclined away from the observer in the northeast. We find that G10.6 is quite different than other young high mass stars in which disk-like molecular structures have been observed (Zhang et al. 1998, 2002; Shepherd & Kurtz 1999; Chini et al. 2004).

2. Observations

We observed the UCHII region G10.6 with the NRAO Very Large Array (VLA)¹ on February 1, 2002, with the phase center at $\alpha(2000) = 18^{\text{h}}10^{\text{m}}28^{\text{s}}.683$, $\delta(2000) = -19^{\circ}55'49''.07$. We observed the (3,3) inversion line of NH_3 at 23.870130 GHz with 63 spectral channels of width 48.828 kHz (0.61 km s^{-1}) for a total bandwidth of 3.125 MHz (38.7 km s^{-1}) centered on $v_{\text{lsr}} = 10 \text{ km s}^{-1}$, and 1.3 cm continuum with a bandwidth of 15.6 MHz. The array was in the A-configuration, yielding a uniform-weighted synthesized beam of width $0.''12 \times 0.''072$ for a physical resolution of $0.0034 \times 0.0021 \text{ pc}$ or $700 \times 430 \text{ AU}$.

We observed the quasars 3C286, 3C273 and 1733-130 for flux, bandpass and phase calibration respectively. Self-calibration of the source amplitudes and phases resulted in a noise level of 0.18 (0.14) mJy beam⁻¹ in the uniform (natural) weighted continuum map, and 1.9 (1.5) mJy beam⁻¹ in each uniform (natural) weighted channel map, about 3 times the thermal noise limit. The images were deconvolved by CLEANing in the usual way with the AIPS task IMAGR. No special steps were taken to deal with the fact that the emission area is much larger than the synthesized beam. The total flux in the resulting natural weighted continuum map is 2.5 Jy, which is consistent with the total flux detected in earlier lower resolution maps of 23 GHz continuum (Keto et al. 1987b). For this reason, we believe that the continuum map is missing very little flux due to the lack of short baselines.

Expressed as a temperature, our sensitivity in a natural weighted continuum map is about 25 K and in a natural weighted channel map is about 280 K. The physical temperature of the molecular gas around G10.6 is estimated to be only 110 K at the ionization front (Keto 1990). Thermal line emission always has a brightness temperature less than the temperature

¹The National Radio Astronomy Observatory is a facility of the National Science Foundation operated under cooperative agreement by Associated Universities, Inc.

of the gas. Thus, the brightest possible thermal emission from the molecular gas would be undetectable, less than 0.4σ . Absorption, however, should be detectable at a wide range of optical depths. The continuum has a peak brightness temperature of 6900 K, and since the noise level in a channel map is 280 K, the molecular line absorption should be detectable at up to 25σ . The quality of the self-calibration solutions and improvements in the K-band receiver system at the VLA have resulted in 25 times better sensitivity in our $\text{NH}_3(3,3)$ channel maps than in the previous best existing $\text{NH}_3(3,3)$ data for this source (Keto et al. 1988), with 3 times better spatial resolution and 2 times better velocity resolution. A sample spectrum is shown in Figure 1.

It should be noted that we have achieved the highest possible angular resolution in studying the problem of high mass star formation. With the VLA in its most extended array configuration, at a frequency of 23 GHz, our spatial resolution is $0''.1$. Imaging thermal (i.e., non-masing) molecular gas at that resolution is only possible toward sources with strong continuum emission, and only at wavelengths which include spectral lines useful for studying the dense gas surrounding UCHII regions. Using radiation with wavelengths around a centimeter is ideal because it is near the peak of the continuum emission from many interesting UCHII regions. At lower frequency, the spatial resolution decreases. At higher frequency the brightness temperature of the continuum emission declines rapidly. So for optimal backlighting from the UCHII region, centimeter wavelengths are ideal. There are few thermal lines associated with high density gas in the centimeter wavelength regime apart from the inversion lines of ammonia which have a critical density of roughly 10^4cm^{-3} (Ho & Townes 1983). In addition to its fortuitous wavelength, the hyperfine structure (one main line, four satellite lines) of the ammonia inversion transitions is extremely useful. Because the different hyperfine components have well-known intrinsic line-strengths, the ratio of the main line to a satellite line can be used to directly calculate the optical depth (what we call hyperfine optical depth) and column density of the ammonia in the rotational state in question, in this case $(J,K) = (3,3)$. While the optical depth of any absorption line can be calculated directly by comparing the depth of the absorption to the strength of the background continuum, this apparent optical depth has limitations. If the filling factor of the absorbing gas is less than one, the apparent optical depth decreases. Also, for deeply embedded objects like G10.6, the main hyperfine component easily saturates. For this reason, the satellite lines, which are much more optically thin and do not saturate easily, are invaluable in investigating the highest optical depths and column densities. Since the hyperfine optical depth is calculated from the ratio of the main line absorption to that of the satellite line, the hyperfine optical depth is accurate even when the main line saturates, and also does not include the effects of the filling factor. The high spatial resolution and sensitivity to high column density gas achieved here have not yet been possible for this sort of object in the millimeter, IR, optical,

or X-ray regimes.

3. Results

We report 6 key observational results. First, we find that the absorbing molecular gas is less spatially extensive than the continuum emission, and, on average, northeast of the average position of the continuum emission. Second, we find that the highest column density gas is localized in clumps, while lower column density gas is seen over the entire face of the UCHII region. Third, we find that the characteristic size scale of the infall-and-rotation kinematic pattern of the molecular gas is larger than the characteristic size scale of the structure in either the optical depth maps, or continuum map. Fourth, we find that the highest optical depth gas is missing on the southwest side of the UCHII region, reinforcing the idea that the absorption is preferentially located in the northeast. Fifth, on size scales smaller than the synthesized beam, i.e. less than $0''.1$ or 500 AU, in more than 75% of the pixels where absorption is detected, the filling factor of the absorbing gas is greater than 0.7. Sixth, none of the sharp edges clearly seen in the continuum emission are seen in maps of the optical depth.

We find that the absorbing molecular gas, as located by the actual line absorption, the apparent optical depth and the hyperfine optical depth, is on average northeast of the continuum emission, and is spatially narrower than the continuum emission in the direction of the minor axis, with the hyperfine optical depth being the most skewed to the northeast, and the most narrow. We have taken slices through the maps shown in Figure 5. The slices run northeast-southwest, and are separated by a synthesized beam-width ($0''.14$). For each slice we have calculated the first moment to determine the mean position of the flux in the maps, and the second moment to determine the width of the flux in the maps. Figures 3 and 4 show the mean positions and widths as a function of position. The origin was chosen so that the mean positions in the continuum map have an average of zero. In the other three maps, the mean positions are generally northeast of the continuum positions. For the hyperfine optical depth map, the mean positions are on average $0''.07$ northeast of the continuum mean positions. Only in slices which pass through the large line-width clump, noted in Figure 5, are the mean positions of the line absorption or apparent or hyperfine optical depth southwest of the continuum positions. The continuum is the widest of the three maps, while the hyperfine optical depth is the narrowest.

We find that the highest column density gas is localized in clumps, while lower column density gas obscures the entire UCHII region. Comparing the two optical depth maps in Figure 5, we note that the hyperfine optical depth map looks “clumpier”. The flux in the

map is mostly collected into peaks about $0''.25$ to $0''.5$ (1500 to 3000 AU) in size, while the apparent optical depth map shows more extended absorption over the whole face of the continuum source. The large line-width clump at the western edge is visible in both maps, as is the clump at the eastern edge. Since the hyperfine optical depth is sensitive to much larger optical depths than the apparent optical depth, we interpret the difference in the maps to imply that, while there is an extended high density envelope, the highest column densities are achieved only in highly localized areas.

We find that the characteristic size scale of the kinematic pattern is much larger than the characteristic size scales of fluctuations in the optical depth or continuum maps. Figure 5 shows the first and second moments of the line absorption in the main hyperfine component. Sollins et al. (2005) has interpreted the bulls-eye pattern in the first moment map as showing simultaneous infall and rotation in a rotating, quasi-spherical, molecular accretion flow. The velocity field appears smooth across the absorption region, with the velocity gradient varying slowly. The size scale of this velocity pattern is visibly much larger than either the size of the continuum structures, or the size of the clumpiness of the optical depth. The clumpiness in the optical depth seems to have no effect on the velocity pattern. The velocity pattern is established for the core as a whole, while the optical depth appears to be picking out overdensities which do not depart from the general flow. The map of the second moment shows that the line width is fairly constant across most of the face of the UCHII region, at around 1.8 km s^{-1} (FWHM = 4.2 km s^{-1}). One spot on the western edge of the UCHII region shows a much larger width, $> 3 \text{ km s}^{-1}$ (FWHM $> 7 \text{ km s}^{-1}$). Interestingly, the bulls-eye pattern in the first moment map shows no real effect of the anomalous large line width clump. That location does not stand out at all in the first moment map, which means that the broadening at this point must be symmetric around a central velocity which fits with the overall velocity field.

The position-velocity cuts highlight both the kinematic pattern seen in the first moment, and also the lack of high optical depth gas in the southwest of the UCHII region. Figure 6 shows two position velocity cuts through the cube of apparent optical depths. The upper panel shows a cut from northwest (negative position) to southeast (positive position). The lower panel shows a cut from southwest (negative position) to northeast (positive position). The largely spherical infall can be seen in the lower panel as a backwards “C” shape. Only the front side of the infall can be detected since we are seeing the line in absorption. In the upper panel, the backwards “C” shape is seen again, but this time tilted, showing the effect of rotation. The lower panel is a cut along the axis of rotation, so only infall is seen. The upper panel is a cut in the plane rotation, so both infall and rotation are seen. In addition, it should be noted that the satellite line can be seen tracing all of the absorption in the upper panel. The satellite appears everywhere in the plane of rotation. But in the lower

panel, the satellite fades out as the cut approaches the southwest side of the UCHII region. The satellite line has an intrinsic line strength of roughly 3% of the main line, so it traces only the highest optical depth gas. Thus the highest optical depth gas is missing on the southwest side of the nebula.

The filling factor of the absorbing gas is large on size scales smaller than a synthesized beam, despite the apparent clumpiness in the optical depth maps. We have noted above that in many pixels, the main line saturates, i.e., in the central channels of the absorption line, there is no detectable flux. When absorbing gas has a non-zero filling factor, the ratio of the depth of the absorption to the continuum strength is related to the optical depth and the filling factor by

$$\frac{T_{line}}{T_{cont}} = \Phi(1 - e^{-\tau}) < \Phi \quad (1)$$

where T_{line} is the depth of the absorption, T_{cont} is the strength of the continuum emission, Φ is the filling factor, and τ is the optical depth. It is impossible to tell the true optical depth when the line has saturated, only a lower limit can be determined. However, the above inequality shows that, no matter what the optical depth is, saturation is only possible where the filling factor is close to one. Furthermore, every measurement of $\frac{T_{line}}{T_{cont}}$ puts a lower limit on Φ . The lower limit on the filling factor is 0.7 in more than 75% of all the points in which main line absorption is detected, and more than 0.9 in 55% of those points.

The sharp-edges of the emission seen in the continuum map are absent in the optical depth maps. The “V” shaped cavity on the northeast side of the UCHII region has very sharp edges, as does the spur to the south. These were interpreted as being the sides of an outflow cavity. The arcs of continuum emission to the east also have sharp edges on the sides facing the UCHII region. These arcs were interpreted by Sollins et al. (2005) as ionized edges of clumps of molecular material. Photons leaking out of the central UCHII region could ionize these clumps externally, naturally creating the arcs, all of which have sharp edges pointing back toward the central source. By contrast, none of the structures in the molecular material have such sharp edges.

4. Discussion

We draw two conclusions from the observational results. First, while the kinematics of the accretion flow are quasi-spherical with slow rotation, the density structure appears flattened and disk-like. Second, the plane of the flattening is inclined to the line of sight.

4.1. The Molecular “Disk”

The densest part of the accretion flow is clearly flattened. The flattening is clear when one compares the apparent optical depth map to the map of the hyperfine optical depth. Figure 5 shows both maps. The hyperfine optical depth, which is sensitive to much higher column densities than the apparent optical depth, is distributed quite narrowly along a line perpendicular to the axis of rotation. Only the large line-width clump in the west deviates from the mid-plane. We have calculated the width of the hyperfine optical depth and the apparent optical depth along 15 slices parallel to the axis of rotation (as described above). Figure 4 shows the widths perpendicular to the disk plane for each of the four maps, continuum, velocity integrated absorption, apparent optical depth, and hyperfine optical depth. Again, the slices which include the large line-width clump stand out. Otherwise, the velocity integrated apparent optical depth, which is sensitive only to lower column density gas, is distributed more broadly, while the velocity integrated hyperfine optical depth, which is sensitive to much higher column densities is narrower. The average 2nd moment of the slices of the continuum map is $0''.36$, for the apparent optical depth map is $0''.23$, and for the hyperfine optical depth map it is $0''.19$. We conclude that the highest density gas is collected in a flattened structure in the mid-plane.

We make three specific predictions of what would be observed if there were a geometrically thin, optically thick accretion disk around G10.6, like those accretion disks seen around low-mass stars. Imagine such a disk-UCHII region system schematically like the planet Saturn and its rings, with the equator inclined relative to the line of sight so that the south pole is visible. (We will discuss the inclination of the rotation axis in G10.6 below) The planet is the UCHII region, the disk is the rings. The northern hemisphere is obscured by the rings, and the southern hemisphere is not. There is a sharp edge to the obscuration, not a gradual edge, where the planet emerges from behind the rings. In the case of a thin-thick molecular disk around a UCHII region, we expect that the molecular absorption will be strong on one side and much weaker on the other. Unlike the case of Saturn’s rings, we do not expect the obscuration to be zero in the southern hemisphere where the disk is behind the UCHII region, because the whole object is embedded in a molecular cloud. But the difference in absorption above and below the disk should be great. Also, if the disk is really geometrically thin compared to the size of the UCHII region, we expect there to be a sharp dividing line between the obscured side and the unobscured side, just like in the Saturn’s rings analogy. Departing from the planet-ring analogy, we can also predict that in a disk-UCHII region system, the absorbing gas in the molecular disk would be well homogenized. Such a disk would only form if the gas were rotationally supported. So the rotation time-scale would be much smaller than the infall time-scale, and any inhomogeneities entering the disk would be quickly smoothed out by differential rotation. The predictions for a thin-thick molecular

disk surrounding an UCHII region are a large difference in optical depths from one side to the other, a sharp dividing line between the two sides, and structurally smooth absorbing material.

G10.6 does not show evidence for a geometrically thin, optically thick disk, and in fact it fits none of our three observational predictions for a thin-thick disk. First, Figure 5 shows that there is very high optical depth gas over most of the face of the UCHII region. While the southwestern edge has less high optical depth gas than the rest, Figure 5 shows no directional preference at all for the apparent optical depth. The only continuum emission without detectable absorption is the southern spur (to which we will return below). Second, there is clearly no sharp dividing line, just a general trend of the higher optical depth gas to be thinner. Third, the absorbing material is inhomogeneous. At our full resolution, the optical depth varies greatly on size scales ($0''.25$) much smaller than the size of the UCHII region ($1 - 2''$), and larger than synthesized beam ($0''.1$). The existence of the arcuate structures to the east has been interpreted as evidence that the surrounding molecular medium is clumpy, and that the arcs are caused by ionizing photons leaking out from the central UCHII region (Sollins et al. 2005). We can confirm the clumpiness of the accretion flow with the optical depth maps, which show variations in integrated optical depth of as much as a factor of eight in a projected distance of less than 1000 AU. While not all of the variations need to be attributed to variations in column density, the other factors which contribute to the optical depth, excitation temperature and ammonia abundance, might not be expected to vary greatly in the molecular gas. The gas distribution in G10.6 is not a geometrically thin, optically thick accretion disk. Instead, the gas is in a flattened, slowly rotating, molecular accretion flow.

Compared to the central mass, the mass of the accretion flow is appreciable. Based on the hyperfine optical depth, and assuming a temperature and ammonia abundance, we can calculate the total molecular mass seen in absorption in the accretion flow. Using 150 K for the excitation temperature of the gas (Sollins et al. 2005), the peak column density of ammonia is greater than $1.2 \times 10^{17} \text{ cm}^{-2}$. This a lower limit because there are points at which the absorption in the satellite line saturates. Our integral over the entire map therefore gives a lower limit. Assuming the ammonia abundance is 10^{-7} relative to H_2 (van Dishoeck & Blake 1998), and adding a factor of 2 since we only detect the front half of the accretion flow in absorption, the total molecular gas mass in the molecular accretion flow is greater than $72 M_{\odot}$. The assumed abundance is the largest source of error here and could be wrong by as much as an order of magnitude in either direction. Using the radius of the UCHII region to set the size scale, the implied mass accretion rate is $0.02 M_{\odot} \text{ yr}^{-1}$. Sollins et al. (2005) calculate that the central mass responsible for the infall is roughly $150 M_{\odot}$. It is entirely possible that the mass of the accretion flow is comparable to the central stellar mass.

The total continuum flux is 2.44 Jy, so assuming constant density, and electron temperature of 10,000 K and a physical size of 8500 AU, the mass of the ionized gas is $0.22 M_{\odot}$. Just by looking at the continuum map it is clear that the density is not uniform, and since we know there is ongoing accretion, the density profile should be proportional to $r^{-3/2}$. The mass, however, depends strongly on the total size of the region in question. So the more spread out ionized gas will dominate the mass. For example, even if we associate all the emission from the marginally resolved peak of the continuum emission with a single density enhancement, the most ionized gas mass we can possibly associate with the peak is $0.0035 M_{\odot}$. Keto (2003) pointed out that, when estimating the Lyman continuum flux necessary to achieve ionization balance, the density gradient can be very important. This is because the recombination rate is proportional to density squared. Because mass is proportional to density only to the first power, the total mass is less sensitive to small high density pockets, and will be dominated by the larger scale structures. Only for a density profile steeper than r^{-2} will the mass be dominated by smaller radii rather than larger radii.

4.2. Inclination of the “Disk”

Sollins et al. (2005) determined that the rotation axis of the molecular accretion flow points northeast when projected into the plane of the sky. Based on our data, the axis of rotation appears to be tipped away from the observer in the northeast. Even though the molecular gas is not in a rotationally supported, geometrically thin disk, the gas distribution is flattened, with denser gas collected in the plane of the equator of the system. Since that plane is tipped, we expect the densest gas to be preferentially in the northeast. We have seen a hint of this already in Figure 6, where the absorption from the main hyperfine component extends right down to the southwest edge of the continuum, while the absorption from satellite component does not. To test for this inclination quantitatively, we have analyzed the maps in Figure 5. For each of the four maps we have made fifteen slices parallel to the axis of rotation, southwest-northeast. Then along each slice we calculate a flux-weighted average position, i.e., the first moment of the slice. In the continuum map, the average positions follow the line closely, and do not systematically deviate in one direction or the other. By contrast, in the hyperfine optical depth map, the average positions are all to the northeast, except at the two points where the anomalous large line-width clump has dragged the average to the southwest. The highest density gas is, on average, $0''.08$ northeast of the projected mid-plane of the continuum, and farther to the northeast if the large line-width clump is excluded. Because the area over which the optical depth can be calculated is defined by the extent of the continuum emission, the mean positions cannot be wildly different. This emphasizes the significance of the offsets in position of the hyperfine optical depth from the

continuum. These offsets are direct evidence that the “disk” is tilted, and the axis of rotation is inclined. Using the radius of the UCHII region, $1''.1$, as a lower limit for the radius of the disk, a $0''.08$ offset is consistent with a tilt of the disk of 4° . Other direct evidence for this inclination has been found by Keto & Wood (2005), who have detected red-shifted $H66\alpha$ emission to the northeast of the UCHII region, within the notch in the continuum emission on that side. They have interpreted that gas as an outflow.

Another clue as to the inclination of the rotation axis is the strength of the absorption on the narrow spurs of continuum. On the northeast side of the continuum source there is the “V”-shaped notch mentioned above. Sollins et al. (2005) interpret this as a possible outflow cavity, and Keto & Wood (2005) have confirmed this. On the southwest side, Keto & Wood (2005) detect no corresponding blue-shifted outflow, but the continuum does show a sharp edged spur, reminiscent of the notch in the northeast. While the spur-like structures in the northeast show strong absorption in both apparent and hyperfine optical depth, the spur in the southwest shows only weak absorption in the apparent optical depth map, and no detectable hyperfine optical depth. This is further evidence that the high density gas in front of the continuum source is in the northeast because of a flattened density profile and the rotation axis being tipped away from the observer in the northeast. However we should note a possible alternate explanation. We cannot rule out the possibility that the southern spur is the limb-brightened edge of a photo-ionized molecular clump, just like the arcs to the east. In that case, the clump might be closer along the line of sight, not physically associated with the main UCHII region, and therefore not obscured by the densest molecular gas.

4.3. A New Phase of Massive Star Formation

The data on G10.6 are unique in the study of accretion onto massive stars because of their spatial resolution, and because the interpretation is not model dependent. Disk-like structures have been detected around a number of very early B type stars. Chini et al. (2004) detected a 10000 AU, morphologically disk-like structure at 550 AU resolution. Kinematic observations at 13000 AU resolution show that the disk is rotating on that larger size scale. In *IRAS* 20126+4104, *IRAS* 18089-1732, AFGL5142, flattening and rotation in dense molecular gas has been detected at roughly 5000 AU resolution. In all three of those cases the sources have infrared luminosities corresponding to early B stars (Zhang et al. 1998, 2002; Beuther et al. 2004). In G192.16-3.82, Shepherd & Kurtz (1999) find a velocity pattern consistent with rotation in water maser spots at a 1000 AU spatial scale, also around an early B star. In all these cases, molecular gas is found to be in rotation, in some cases apparently Keplerian rotation, around early B type or even late O type stars. All are consistent with the existence

of rotating, molecular accretion disks which, in many respects, are larger versions of the disks observed around low-mass protostars. In contrast to previous work, in G10.6 we have 500 AU physical resolution in the thermally emitting molecular gas. The spatial resolution is enough to completely resolve the motions involved. The kinematics and optical depths are fairly unambiguous. The densest gas is flattened, and the velocities clearly show infall and slow rotation.

G10.6 itself contrasts with objects from previous massive-star-disk studies in that it cannot be interpreted as a scaled up version of low-mass star formation. All the cases cited above (*IRAS* 20126, *IRAS* 18089, G192.16, M17, and AFGL5142) are consistent with the central object being a single stellar system of up to $20 M_{\odot}$. In most of these objects the existence of a bipolar outflow indicates ongoing accretion. The analogy to the formation mechanisms of low-mass stars is fairly straightforward, scaled up in size and mass, although a key difference is ratio of disk mass to stellar mass, small for low mass stars, but apparently large for high mass stars. In G10.6, the central source is at least $150 M_{\odot}$, close to $10^6 L_{\odot}$, and is almost certainly not a single star or binary. At the edge of the UCHII region, at a radius of 5000 AU, the molecular gas is clearly moving inward, and Keto (2002a) detect inward motions in the ionized gas down to radii of less than 1000 AU. While we cannot say how or if the inward moving gas actually accretes onto one or more of the central stars, we can say with great certainty that inward motion continues in the molecular gas from the 0.5 pc scale (Ho & Haschick 1986; Keto et al. 1988) down to thousands of AU. This is a single continuous accretion flow traceable over two orders of magnitude in size, toward a group of young massive stars. This suggests a completely different phase or mode of star formation than that seen in low mass stars, or in the preceding examples of individual massive young stars.

5. Summary

We have utilized the strong 23 GHz radio continuum emission from the UCHII region G10.6-0.4 to serve as a backlight for examining the foreground molecular material seen in absorption. Using the VLA, we have achieved very high angular ($0''.1$) and spatial (500 AU) resolution. In the past, such resolutions have not been possible for studying the circumstellar environment of massive young stars. Making use of the hyperfine structure of the $\text{NH}_3(3,3)$ inversion line, we are sensitive to optical depths of up to 80. This allowed us to investigate the structure of the densest circumstellar material. We find that in the densest material, the structure is flattened, with an aspect ratio of 5. The structure is displaced with respect to the mean continuum emission, consistent with a tilt of the disk along the line of sight at 4° ,

away from the observer in the northeast. The flattened structure has a mass of $72 M_{\odot}$, much larger than the ionized gas in the HII region of $0.2 M_{\odot}$. The velocity pattern within the circumstellar material, as well as its clumpiness, suggest a dynamically collapsing structure which is not centrifugally supported. The implied infall rate is very high, on the order of $0.02 M_{\odot}\text{yr}^{-1}$. The kinematics of the circumstellar material, which agree with the kinematics of the ionized gas within the HII region, suggest that this infalling material continues across the ionization front. Because we do not know how much mass is actually being accreted by the stars, or how much mass is leaving the system in the outflow, it is impossible to know for sure whether G10.6 is in quasi-static equilibrium, or if it is evolving dynamically. However, the very high mass and luminosity involved mean that this is a different type of object than the individual high-mass protostars which have been investigated in the past.

The authors would like to acknowledge Eric Keto and Qizhou Zhang for their helpful comments and suggestions in the preparation of this paper.

REFERENCES

- Argon, A. L., Reid, M. J., & Menten, K. M. 2000, *ApJS*, 129, 159
- Beuther, H., Hunter, T. R., Zhang, Q., Sridharan, T. K., Zhao, J.-H., Sollins, P., Ho, P. T. P., Ohashi, N., Su, Y. N., Lim, J., & Liu, S.-Y. 2004, *ApJ*, 616, L31
- Braz, M. A. & Epchtein, N. 1983, *A&AS*, 54, 167
- Casoli, F., Combes, F., Dupraz, C., Gerin, M., & Boulanger, F. 1986, *A&A*, 169, 281
- Chini, R., Hoffmeister, V., Kimeswenger, S., Nielbock, M., Nürnberger, D., Schmidtobreick, L., & Sterzik, M. 2004, *Nature*, 429, 155
- Downes, D., Wilson, T. L., Bieging, J., & Wink, J. 1980, *A&AS*, 40, 379
- Ho, P. T. P. & Haschick, A. D. 1986, *ApJ*, 304, 501
- Ho, P. T. P., Terebey, S., & Turner, J. L. 1994, *ApJ*, 423, 320
- Ho, P. T. P. & Townes, C. H. 1983, *ARA&A*, 21, 239
- Hofner, P. & Churchwell, E. 1996, *A&AS*, 120, 283
- Hofner, P., Wyrowski, F., Walmsley, C. M., & Churchwell, E. 2000, *ApJ*, 536, 393
- Keto, E. 2002a, *ApJ*, 568, 754

- . 2002b, *ApJ*, 580, 980
- . 2003, *ApJ*, 599, 1196
- Keto, E. & Wood, K. 2005, *ApJ*, 0, 1
- Keto, E. R. 1990, *ApJ*, 355, 190
- Keto, E. R., Ho, P. T. P., & Haschick, A. D. 1987a, *ApJ*, 318, 712
- . 1988, *ApJ*, 324, 920
- Keto, E. R., Ho, P. T. P., & Reid, M. J. 1987b, *ApJ*, 323, L117
- Mueller, K. E., Shirley, Y. L., Evans, N. J., & Jacobson, H. R. 2002, *ApJS*, 143, 469
- Plume, R., Jaffe, D. T., & Evans, N. J. 1992, *ApJS*, 78, 505
- Shepherd, D. S. & Kurtz, S. E. 1999, *ApJ*, 523, 690
- Sollins, P. K., Ho, P. T. P., Keto, E., & Zhang, Q. 2005, *ApJ*, 630, L1
- Spitzer, L. 1978, *Physical processes in the interstellar medium* (New York Wiley-Interscience, 1978. 333 p.)
- Strömgren, B. 1939, *ApJ*, 89, 526
- van Dishoeck, E. F. & Blake, G. A. 1998, *ARA&A*, 36, 317
- Walsh, A. J., Burton, M. G., Hyland, A. R., & Robinson, G. 1998, *MNRAS*, 301, 640
- Wood, D. O. S. & Churchwell, E. 1989, *ApJ*, 340, 265
- Zhang, Q., Hunter, T. R., & Sridharan, T. K. 1998, *ApJ*, 505, L151
- Zhang, Q., Hunter, T. R., Sridharan, T. K., & Ho, P. T. P. 2002, *ApJ*, 566, 982

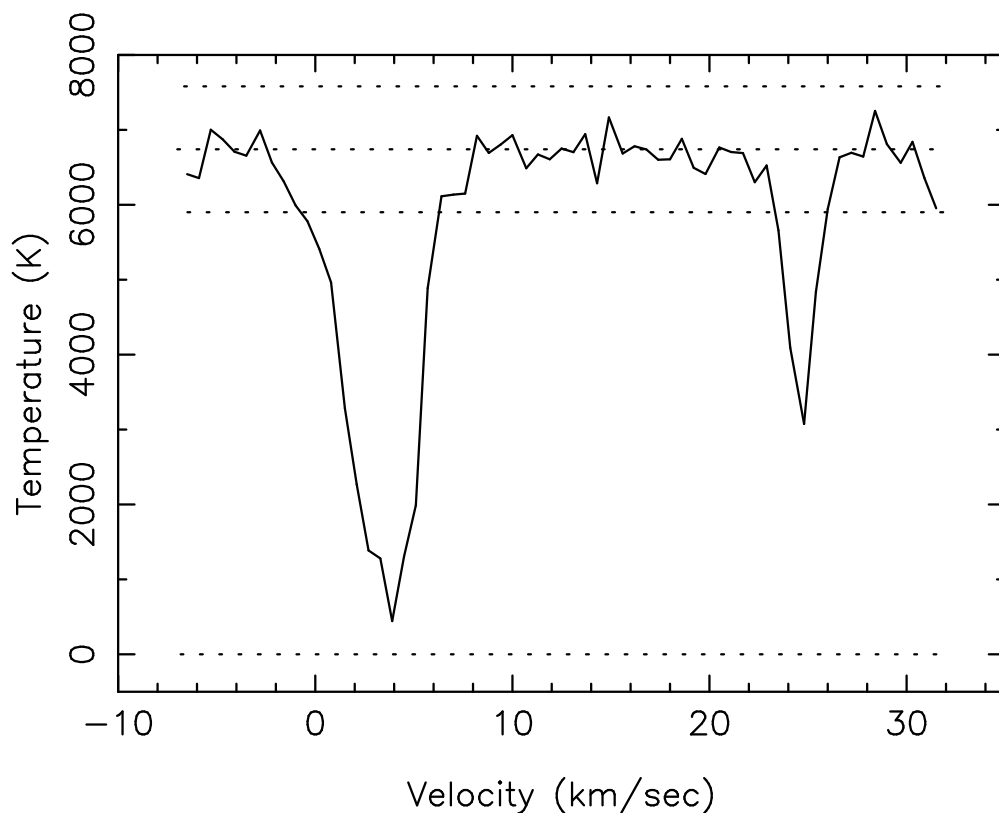


Fig. 1.— A sample spectrum of the $\text{NH}_3(3,3)$ line from near the peak of the continuum emission. The dotted lines show the continuum level, here 6700 K, the continuum plus and minus 3σ , and zero. The first satellite line is clearly visible, but the outer satellite is out of the spectral window.

Fig. 2.— The continuum map and the maps of the zeroth moments of the line absorption, the apparent optical depth of the main hyperfine component, and the hyperfine optical depth. In all four frames, the contour is the 1 mJy beam^{-1} continuum level. The color-scales are all linear, running from -1 to 45 mJy beam^{-1} for the continuum, from 5 to $-200 \text{ mJy beam}^{-1} \text{ km s}^{-1}$ for the line absorption, from 0 to 14 km s^{-1} for the apparent optical depth, and from 0 to 320 km s^{-1} for the hyperfine optical depth. Notice that the apparent optical depth is seen over the entire face of the continuum source, while the hyperfine optical depth is concentrated in a thin strip in the plane of rotation. The units of the optical depth maps here are km s^{-1} because optical depth itself is unitless, while the maps are of optical depth integrated over velocity.

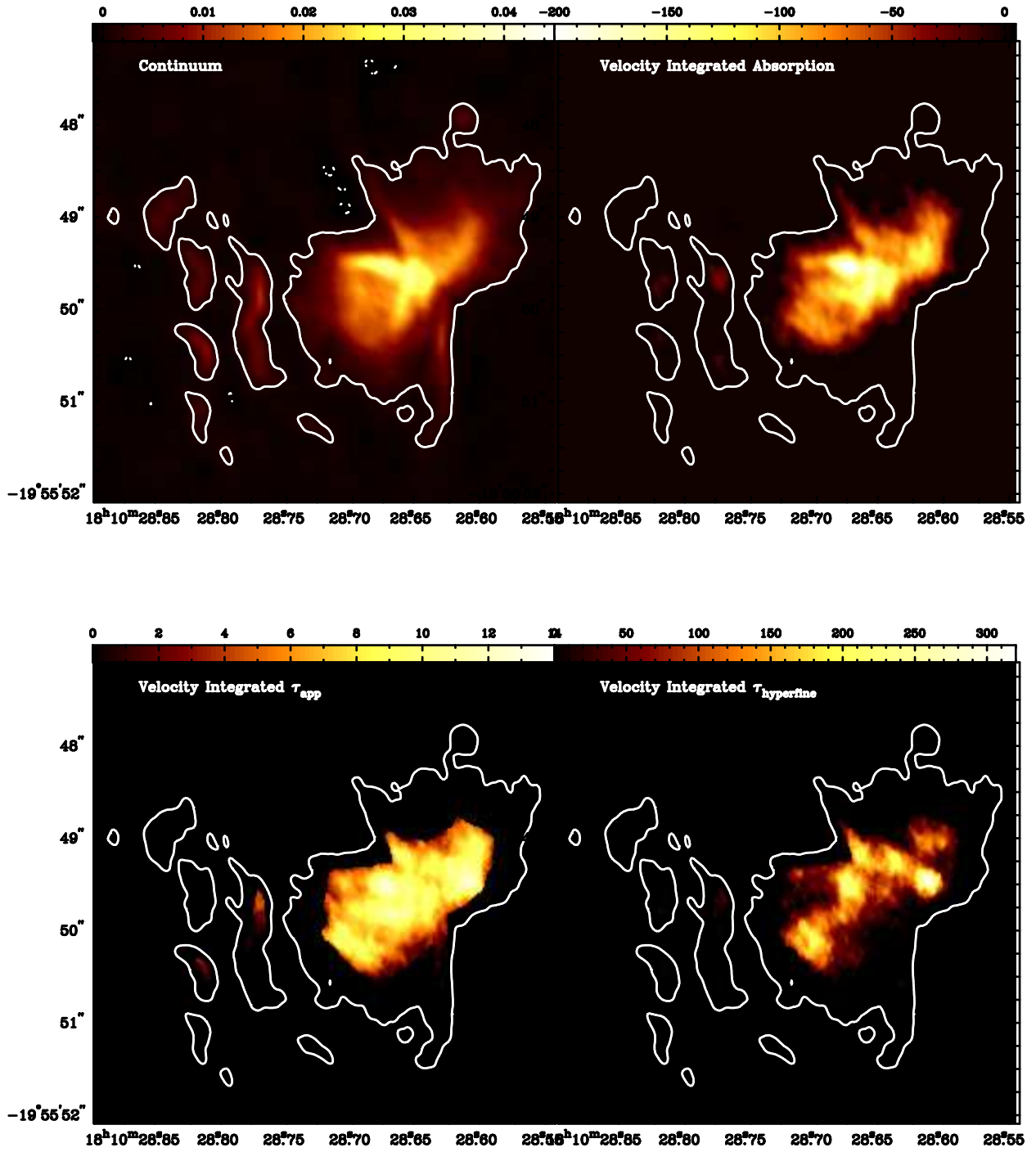


Fig. 2.— Continued

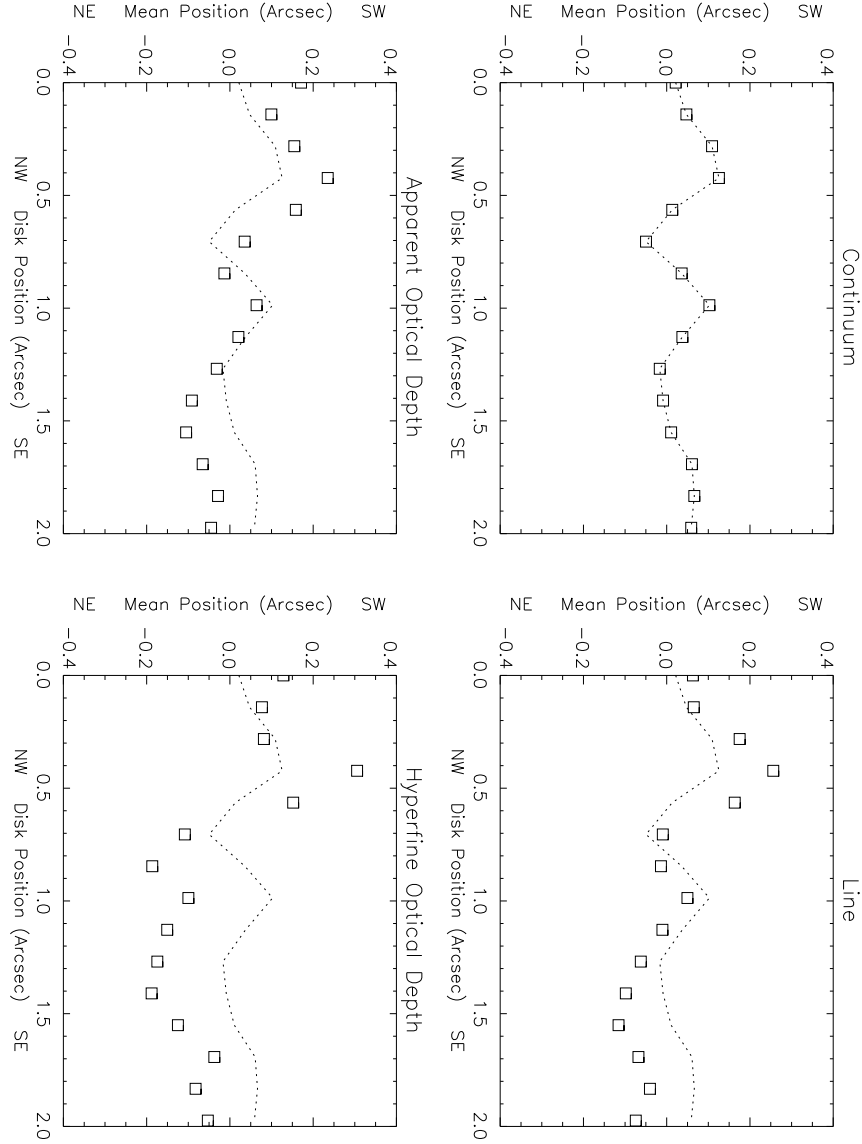


Fig. 3.— Plots of the mean position of the flux in the continuum map and the velocity integrated line, apparent optical depth, and hyperfine optical depth maps relative to the mid-plane of the UCHII region. The squares are the mean positions, while the dotted line shows the continuum mean positions for reference. In integrating over velocity only the main hyperfine component is included. Except for the position of the large line-width clump, the hyperfine optical depth mean positions are northeast of the mid-plane. The apparent optical depth and the raw absorption line have mean positions closer to the continuum mean positions.

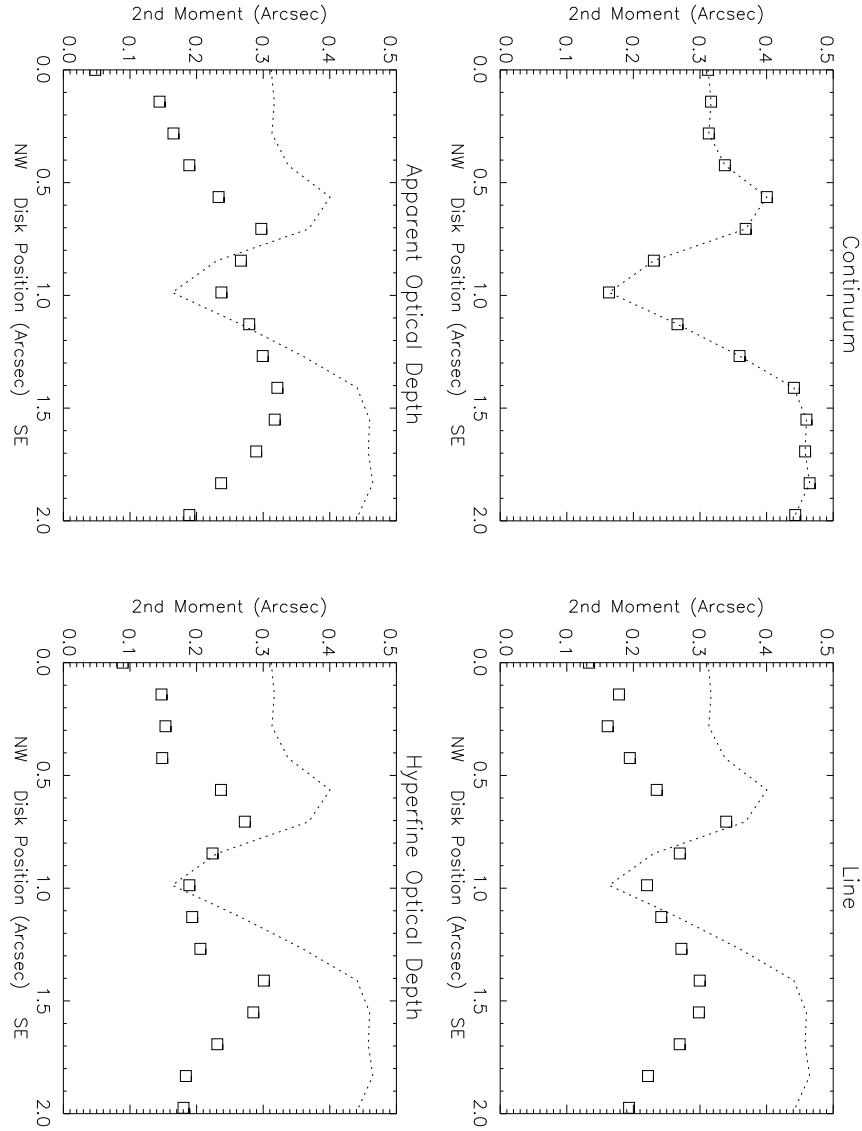


Fig. 4.— Plots of the second moment of the flux in slices of the continuum map and the velocity integrated line, apparent optical depth, and hyperfine optical depth maps relative to the mid-plane of the UCHII region. The squares are the widths while the dotted line is widths of the continuum, plotted for reference. In integrating over velocity only the main hyperfine component is included. The emission is always narrowest near the outflow cavities where the continuum is “pinched”. The hyperfine optical depth is the narrowest.

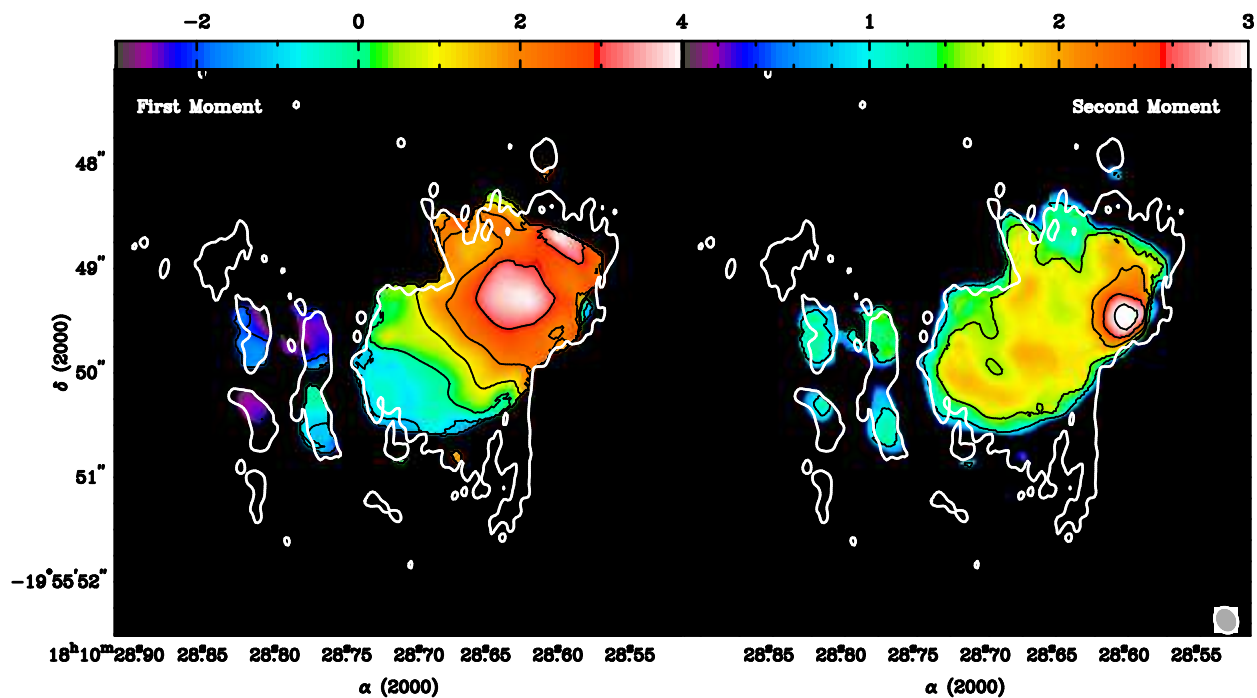


Fig. 5.— The map of the first (left) and second (right) moments of the main hyperfine component of the $\text{NH}_3(3,3)$ line with one contour from the continuum map. For the first moment, the colors range from $v_{\text{lsr}} = -3$ to $+4$ km s^{-1} . For the second moment, the colors range from 0 to 3 km s^{-1} . For a pure Gaussian line, the full width of half-maximum is 2.35 times the second moment. The contour, shown for reference, is the 0.8 mJy beam^{-1} contour from the 1.3 cm continuum map. The line data were mapped by the AIPS task IMAGR with natural weighting and a u-v taper at 750 kilolambda so that the resulting synthesized beam ($0.''26 \times 0.''22$) better matched the size scale of velocity pattern.

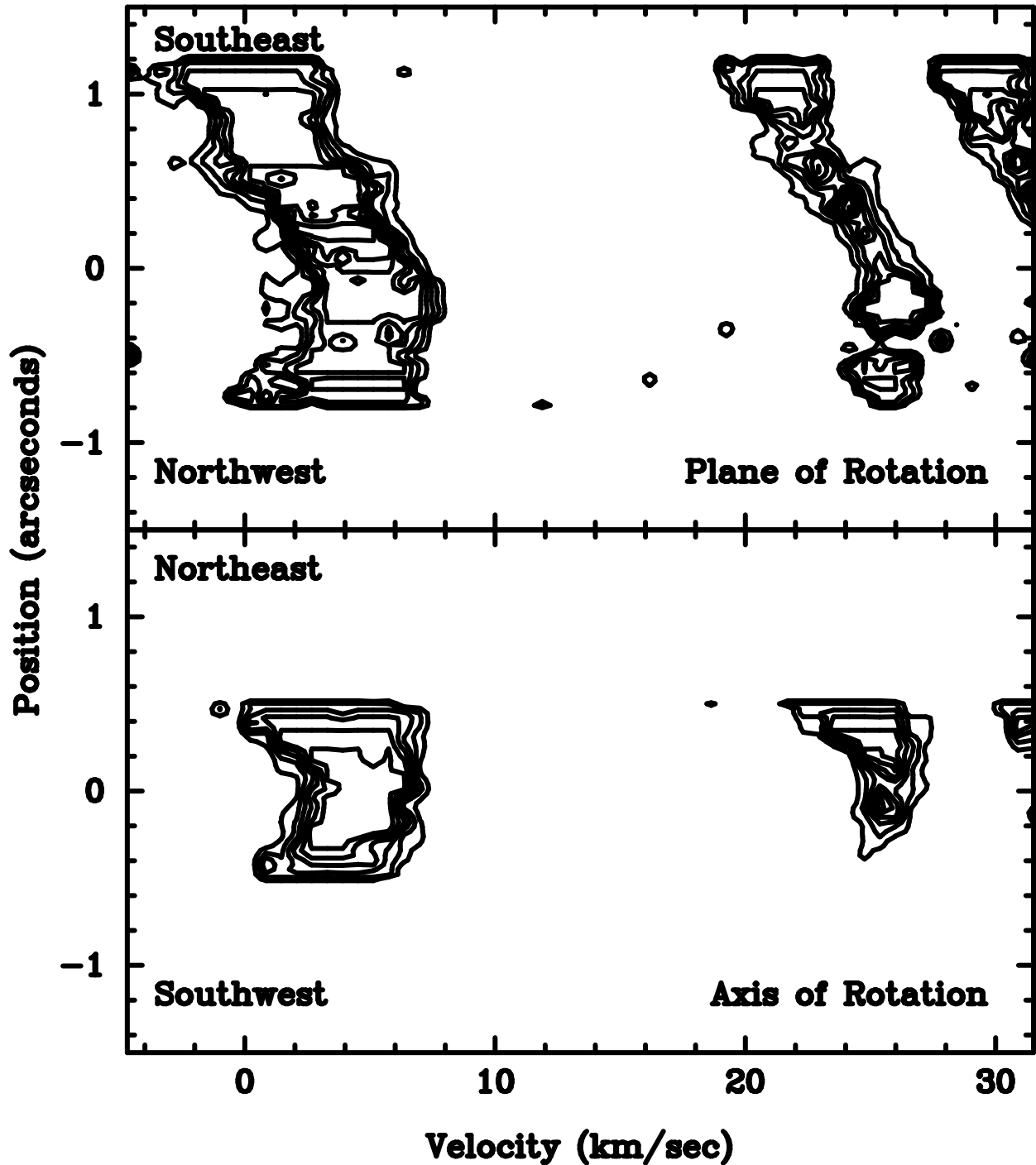


Fig. 6.— Position velocity diagrams of two cuts through the cube of apparent optical depths of the $\text{NH}_3(3,3)$ line. The contours are at $\tau = 1, 2, 3, 4, 5, 6, 7, 8, 9, 10 \times 0.3$. Notice that in the plane of rotation, the satellite has roughly constant optical depth at all positions. Along the axis of rotation however, the satellite line fades out in the southwest indicating the presence of higher density gas in the northeast. This is due to the inclination of the rotation axis to the line of sight.